BEST AVAILABLE IMAGES

Defective images within this document are accurate representations of the original documents submitted by the applicant.

Defects in the images may include (but are not limited to):

- BLACK BORDERS
- TEXT CUT OFF AT TOP, BOTTOM OR SIDES
- FADED TEXT
- ILLEGIBLE TEXT
- SKEWED/SLANTED IMAGES
- COLORED PHOTOS
- BLACK OR VERY BLACK AND WHITE DARK PHOTOS
- GRAY SCALE DOCUMENTS

IMAGES ARE BEST AVAILABLE COPY.

As rescanning documents *will not* correct images, please do not report the images to the Image Problem Mailbox.

Forced Convection in High Porosity Metal Foams

V. V. Calmidi[1]

R. L. Mahajan

CAMPmode,
Department of Mechanical Engineering,
University of Colorado at Boulder,
Boulder, CO 80309-0427

This paper reports an experimental and numerical study of forced convection in high porosity (ε~0.89–0.97) metal foams. Experiments have been conducted with aluminum metal foams in a variety of porosities and pore densities using air as the fluid medium. Nusselt number data has been obtained as a function of the pore Reynolds number. In the numerical study, a semi-empirical volume-averaged form of the governing equations is used. The velocity profile is obtained by adapting an exact solution to the momentum equation. The energy transport is modeled without invoking the assumption of local thermal equilibrium. Models for the thermal dispersion conductivity, k_d, and the interstitial heat transfer coefficient, h_{sf}, are postulated based on physical arguments. The empirical constants in these models are determined by matching the numerical results with the experimental data obtained in this study as well as those in the open literature. Excellent agreement is achieved in the entire range of the parameters studied, indicating that the proposed treatment is sufficient to model forced convection in metal foams for most practical applications. [S0022-1481(00)01903-4]

Keywords: Convection, Experimental, Heat Transfer, Porous Media, Thermal

Introduction

Forced and buoyancy-induced convection in porous media have been studied extensively for over 50 years (see Kaviany [1] for a good review on the subject). However, most studies in this category have been restricted to packed beds and granular materials, since they have direct application to naturally occurring porous media, with porosities in the range 0.4–0.6. As discussed below, there are relatively few investigations of transport phenomena in very high porosity media (ε>0.9) such as metal foams.

Only during the last ten years, transport phenomena in metal foams have started to receive attention ([2–6]). Hunt and Tien [2] studied forced convection in metal foams with water as the fluid phase. Using the technique of volume averaging, and under the simplifying assumption of local thermal equilibrium, they showed that a single energy equation could adequately describe forced convection in metal foams. Sathe et al. [3] studied combustion in metal foams as applied to porous radiant burners. Lee et al. [4] studied the application of metal foams as high-performance air-cooled heat sinks in electronics packaging. In their experimental study, they demonstrated that a 1 cm^2 chip dissipating 100 W could be cooled using an aluminum foam heat sink, and a low-power muffin fan. Recently, Calmidi and Mahajan [5] addressed heat conduction in aluminum metal foams. They obtained experimental data and developed an analytical model for the thermal conductivity, taking into account the open-celled structure of metal foams. Bhattacharya et al. [6] extended that work to cover a wider range of solid to fluid conductivity ratios. Further, the analytical model was refined to address issues of isotropicity.

Our review suggests that there are no thermal transport studies in the literature (pertaining to high porosity metal foams) that (a) employ experimentally validated thermal conductivity data, (b) consider local thermal nonequilibrium among phases, and (c) accurately consider metal foam microstructure. The focus of this paper is to take these factors into account.

Metal foams (Fig. 1) can be broadly classified as porous media in which the medium has a distinct but continuous and rigid solid phase, and a fluid phase. They are typically available in high porosities (ε>0.9). They also have a unique open-celled structure. As a result, most of the past studies on packed beds, and granular porous media are not applicable to metal foams. There is thus a need to develop a fundamental understanding of the transport phenomena in these foams. As shown later in this paper, both numerical and experimental studies are currently needed to generate heat transfer information for practical applications.

Energy transport in porous media has generally been studied with the assumption of local thermal equilibrium among the two phases. That is, a single homogeneous equation is used to describe transport with the assumption that the solid and fluid phases have the same temperature field. Following such an assumption, the effective stagnant thermal conductivity, k_e, of a porous medium is used to account for the solid and fluid phase conductivities. The stagnant conductivity k_e, is sometimes augmented by the dispersion conductivity, k_d. Dispersion is a hydrodynamic phenomenon which becomes prominent at high Reynolds numbers, especially if k_e is small in magnitude. Several empirical and analytical studies have attempted to quantify dispersion in porous and fibrous media ([2,7–9]). The general conclusion is that at high Peclet numbers, k_d is linearly proportional to the local flow velocity.

Under certain situations, however, the assumption of local thermal equilibrium has to be relaxed. Such a condition might arise when there is internal heat generation ([3]) or when the difference in the stagnant conductivities of the solid and the fluid phases is significant. The latter situation is encountered when metal foams are used with low-conductivity fluids like air or water. With local thermal nonequilibrium, the solid and fluid temperature fields have to be obtained separately. In addition, appropriate coupling is necessary between the solid and fluid phase energy equations to account for the interfacial heat transfer.

The focus of this study is forced convection in metal foams. First, the experimental method used to obtain Nusselt number data for a number of aluminum metal foam samples with air as the fluid medium is described. Following a discussion of the appropriate form of the governing equations of momentum and energy in metal foams, the details on the numerical method used to solve them are provided. Finally, the numerical results are compared with the experimental data to obtain values of empirical constants

[1]To whom correspondence should be addressed. Currently at the Advanced Thermal Engineering Laboratory, IBM Microelectronics, 1701 North Street, Endicott, NY 13760.

Contributed by the Heat Transfer Division for publication in the JOURNAL OF HEAT TRANSFER. Manuscript received by the Heat Transfer Division, May 17, 1999; revision received, Feb. 14, 2000. Associate Technical Editor: R. Douglass.

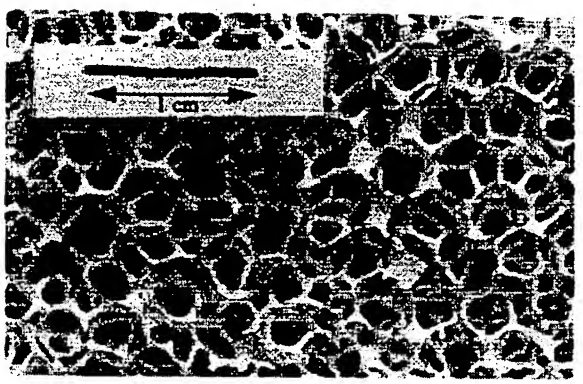

Fig. 1 Picture of a typical metal foam sample

in the thermal dispersion and the interfacial heat transfer coefficient models.

Experiment

A schematic of the experimental setup is shown in Fig. 2. Aluminum metal (alloy T-6201) foam samples of size 63 mm×45 mm×196 mm were used in the experiments. Table 1 lists the characteristics of the samples that were used in the experiment. The porosity is the void volume fraction and the pore density is the number of pores per unit length of the material (PPI, pores per inch) and, d_f and d_p are the average fiber diameter and pore diameter, respectively. The porosity of each sample was estimated using the weight of a given volume of the sample and the density of aluminum alloy T-6201. The fiber diameter, d_f, was measured using a microscope, and the pore diameter, d_p, was estimated by counting the number of pores in a given length of material. Both d_f and d_p are average values. The pore density (PPI) is a nominal value supplied by the manufacturer.

For each experimental run, a metal foam sample was placed in a plexiglass tube. Air flow was achieved by connecting the plexiglass tube to a fan/motor assembly (not shown in figure) downstream of the test sample. The direction of air flow is from left to right as shown in Fig. 2. Very low conductivity styrofoam was used to block the space around the sample to fully prevent flow bypass. A pressure transducer was used to measure the pressure drop across the metal foam sample. An orifice plate was used to measure the flow rate through the metal foam sample.

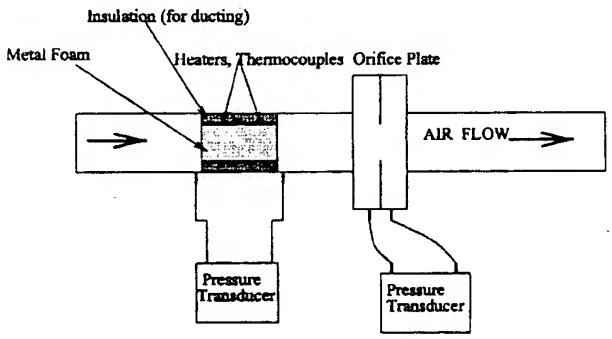

Fig. 2 Schematic of the experimental setup used for the forced convection experiments

The metal foam samples were brazed to 9.5-mm thick aluminum skins on two sides. On one of the skins, grooves were cut to isolate a section of the metal foam. Patch heaters were fixed to this isolated portion of the skin between the grooves (Fig. 3). The resulting physical dimensions of the heated section of the metal foam are 63 mm×45 mm×114 mm. The grooves in the skin were loosely filled with insulating material to prevent conduction losses from the heated to the unheated sections. Then, two thin (2-mm) grooves were cut in the metal foam below the grooves on the skin (Fig. 3). This was done to prevent back-conduction of heat from the heated to the unheated sections. This isolating scheme ensures that fully developed flow enters the heated section of the metal foam (Calmidi [10]). Six 36-gage T-type thermocouples (axial thermocouples) were fixed along axial locations in the skin as shown in Fig. 3. For some samples, two thermocouples were fixed at off-center locations (25 mm from the center). Two additional thermocouples were used to monitor the ambient temperature and the temperature of the air at the midplane before it entered the heated section. The total flow rate was estimated according to ASME/ISO-5167-1:1991 using the pressure drop across the orifice plate as well as the temperature and pressure of the air entering the orifice plate. The average velocity (superficial) of air flowing through the metal foam, u_o, is then the average flow rate divided by the area of cross section.

During a typical experiment run, the speed of the motor was adjusted such that the flow velocity was set at a desired value. The power input to the patch heaters was set between 15–35 W. The temperature readings indicated by the thermocouples were monitored until they reached steady state. This took approximately 5–10 minutes depending on the flow velocity. It typically took longer at lower flow velocities. The temperatures were monitored for an additional interval of five minutes to ensure that steady state had indeed been reached. Steady state was assumed if the temperature did not vary more than 0.1°C during a five-minute interval. The temperature readings of all the thermocouples with respect to the ambient temperature were noted. The temperature variation along the axis (x-direction) was within 15 percent of the average value, while the temperature variation perpendicular to the axis (z-direction) was less than 0.1°C in all the experimental runs. The air temperature before it entered the heated section (T_{in}) was also measured. It was slightly higher than the ambient temperature (T_{amb}), but always less than two percent of the maximum wall temperature, indicating that back-conduction effects were negligible. Figure 4 shows the data (wall temperature variation) collected from a typical experiment for Sample 2 (Table 1). The data collected for all the samples is documented in Calmidi [10].

Using the measured wall temperature data, the heat flux is con-

Table 1 Characteristics of metal foam samples used in experimental study

#	Porosity	PPI	d_f (m) Fiber Dia.	d_p (m) Pore Dia.	f	K ($*10^7$ m^2)	k_{se} (W/m-K)	k_{fe} (W/m-K)
1	0.9726	5	0.00050	0.00402	0.097	2.7	2.48	0.0256
2	0.9118	5	0.00055	0.00380	0.085	1.8	6.46	0.0237
3	0.9486	10	0.00040	0.00313	0.097	1.2	4.10	0.0248
4	0.9546	20	0.00030	0.00270	0.093	1.3	3.71	0.0250
5	0.9005	20	0.00035	0.00258	0.088	0.9	7.19	0.0233
6	0.9272	40	0.00025	0.00202	0.089	0.61	5.48	0.0242
7	0.9132	40	0.00025	0.00180	0.084	0.53	6.37	0.0237

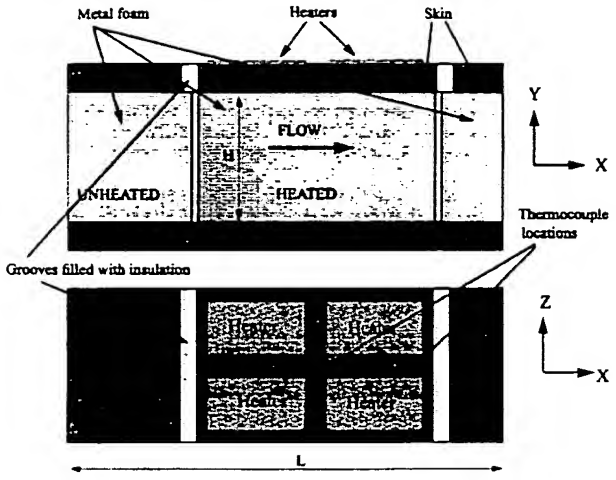

Fig. 3 Schematic of side and top views of metal foam samples used in the experiments

verted into an average Nusselt number. The average temperature ΔT_{avg} is defined as the average of the six values of the temperature measured. That is,

$$\Delta T_{avg} = \left(\sum_{i=1}^{n} T_{wi} \right) \Big/ n - T_{in} \tag{1}$$

where n is the number of points where the wall temperature was measured. It is noted that, although this value is not the actual average wall temperature, it does represent an appropriate scale to represent the temperature difference. Next an average heat transfer coefficient is defined as

$$\bar{h} = q/(A\Delta T_{avg}) \tag{2}$$

where q is the power input to the heaters and A is the area of cross section of the metal foam. From this, an average Nusselt number is calculated using

$$\mathrm{Nu} = \bar{h}L/k_e \tag{3}$$

where L is the length of the heated section of the metal foam, and k_e is the effective thermal conductivity $(k_{fe}+k_{se})$ as given in Table 1.

The effect of varying the power input to the heaters was also investigated to verify that nonlinear effects like buoyancy, radiation, and property variation were negligible. In all cases studied, the Nusselt number was found to be nearly independent of the input power.

The experimental error estimate can be made based on the accuracies in the measurement of the individual quantities. The error (thermocouple calibration and resolution of the data acquisition device) in the estimation of ΔT_{avg} is 0.3°C. Based on the published accuracies of the voltmeter and ammeter, the error in the estimate of q is two percent. The errors in the estimate of the length and area are neglected because they are extremely low (<0.3 percent of the measured quantity). Based on these values, the error in the estimate of the Nusselt numbers is 4.3 percent. This estimate is based on a representative value of ΔT_{avg} of 8°C. Based on the accuracy of the pressure transducers, the error in the estimate of the velocity is 4.1 percent.

Analysis

The steady volume-averaged momentum equation that governs fluid flow in porous media is given by

$$\frac{\rho}{\varepsilon^2}\nabla\cdot\mathbf{uu} = -\nabla p + \frac{\mu}{\varepsilon}\nabla^2\mathbf{u} - \frac{\mu}{K}\mathbf{u} - \frac{\rho f}{\sqrt{K}}\|\mathbf{u}\|\mathbf{u}. \tag{4}$$

In Eq. (4), the drag due to the fibers is represented by the familiar non-Darcy formulation. The third term on the R.H.S. of Eq. (4) is the traditional Darcy term which is used to account for the pressure drop due to viscous friction at the walls of the fibers, and the fourth term is the nonlinear correction and represents the pressure drop due to the form drag and the flow separation that takes place at higher Reynolds numbers. A linear superposition of the two terms as shown here is semi-empirical, but has been known to match experimental data in many situations ([2,8,11–13]). A modified form of Eq. (4) was used by Calmidi [10], Chapter 3, to determine the permeability, K, and the inertia coefficient, f, of the metal foam samples. These are listed in Table 1.

The energy equations for the solid and the fluid phases based on thermal nonequilibrium are

$$0 = \frac{\partial}{\partial x}\left(k_{se}\frac{\partial T_s}{\partial x}\right) + \frac{\partial}{\partial y}\left(k_{se}\frac{\partial T_s}{\partial y}\right) - h_{sf}a_{sf}(T_s - T_f) \tag{5}$$

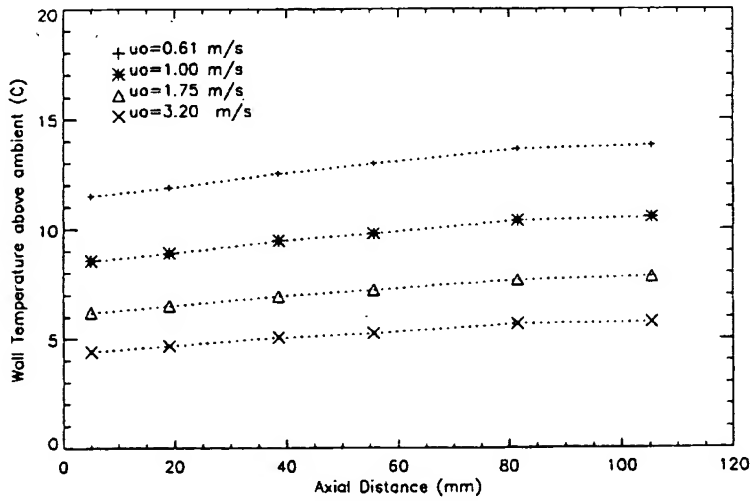

Fig. 4 Variation in wall temperature with average flow velocity (Sample 2, Table 1)

$$(\rho c_p)_f u \frac{\partial T_f}{\partial x} = \frac{\partial}{\partial x}\left((k_{fe}+k_d)\frac{\partial T_f}{\partial x}\right) + \frac{\partial}{\partial y}\left((k_{fe}+k_d)\frac{\partial T_f}{\partial y}\right) + h_{sf}a_{sf}(T_s - T_f). \quad (6)$$

The coupling between the two equations is achieved using the interfacial term which represents the heat transfer between the two phases via a heat transfer coefficient, h_{sf}, and the specific surface area, a_{sf}. It is important to note that Eqs. (5), and (6) are semi-empirical and are not the full volume-averaged forms of the energy equations ([14,15]). The full volume-averaged treatment is considerably complex, and has been solved exactly only for a one-dimensional system of parallel capillary tubes ([16]). However, it is noted that the semi-empirical treatment employed here has been successfully used in the past to model transport in beds of spheres ([17,18]).

An analytical model for obtaining the effective conductivity of metal foams has been derived in ([5]). Their experimentally validated model was based on the structure of metal foams. It is reproduced as

$$k_e = \left(\left(\frac{2}{\sqrt{3}}\right)\left(\frac{r\left(\frac{b}{L}\right)}{k_f + \left(1+\frac{b}{L}\right)\frac{(k_s-k_f)}{3}} + \frac{(1-r)\left(\frac{b}{L}\right)}{k_f + \frac{2}{3}\left(\frac{b}{L}\right)(k_s-k_f)} + \frac{\frac{\sqrt{3}}{2}-\frac{b}{L}}{k_f + \frac{4r}{3\sqrt{3}}\left(\frac{b}{L}\right)(k_s-k_f)}\right)\right)^{-1} \quad (7)$$

where $r = 0.09$, and the ratio b/L is given by

$$\frac{b}{L} = \frac{-r + \sqrt{r^2 + 4(1-\varepsilon)\frac{\sqrt{3}}{2}\left(\left(2 - r\left(1+\frac{4}{\sqrt{3}}\right)\right)\Big/ 3\right)}}{\frac{2}{3}\left(2 - r\left(1+\frac{4}{\sqrt{3}}\right)\right)}. \quad (8)$$

The solid-phase conductivity, k_{se}, is obtained by setting $k_f = 0$, in Eq. (7). By doing so

$$k_{se} = \left(\left(\frac{2}{\sqrt{3}}\right)\left(\frac{r\left(\frac{b}{L}\right)}{\left(1+\frac{b}{L}\right)\frac{k_s}{3}} + \frac{(1-r)\left(\frac{b}{L}\right)}{\frac{2}{3}\left(\frac{b}{L}\right)k_s} + \frac{\frac{\sqrt{3}}{2}-\frac{b}{L}}{\frac{4r}{3\sqrt{3}}\left(\frac{b}{L}\right)k_s}\right)\right)^{-1}. \quad (9)$$

Similarly, k_{fe} is obtained by setting $k_s = 0$ in Eq. (7),

$$k_{fe} = \left(\left(\frac{2}{\sqrt{3}}\right)\left(\frac{r\left(\frac{b}{L}\right)}{k_f + \left(1+\frac{b}{L}\right)\frac{(-k_f)}{3}} + \frac{(1-r)\left(\frac{b}{L}\right)}{k_f + \frac{2}{3}\left(\frac{b}{L}\right)(-k_f)} + \frac{\frac{\sqrt{3}}{2}-\frac{b}{L}}{k_f + \frac{4r}{3\sqrt{3}}\left(\frac{b}{L}\right)(-k_f)}\right)\right)^{-1}. \quad (10)$$

Values of k_{se} and k_{fe} obtained using Eqs. (9) and (10) are listed in Table 1.

In Eqs. (5) and (6), the dispersion conductivity is assumed to be isotropic. That is

$$k_{dx} = k_{dy} = k_d. \quad (11)$$

Based on earlier work ([2,7]), the following model is proposed for the dispersion conductivity:

$$\frac{k_d}{k_e} = C_D(\mathrm{Re}_K \mathrm{Pr}_e)\frac{u}{u_o}. \quad (12)$$

In Eq. (12), the coefficient of thermal dispersion, C_D, remains to be determined. As a simplification, this model for k_d does not account for wall effects ([19,20]) except through the change in the velocity profile near the wall.

One of the most comprehensive models for the interfacial heat transfer coefficient, h_{sf}, for packed beds is by Wakao et al. ([17]). For foamed materials, however, no such general model exists. However, the radial temperature gradients within the fibers are expected to be small and it is reasonable to use the Nusselt number correlation for external flow over a body of an appropriate cross section. Based on a correlation developed by Zukauskas [21] for cylinders in crossflow in the range of Reynolds numbers (40–1000), a model for the interfacial heat transfer is proposed as follows:

$$\mathrm{Nu}_{sf} = \frac{h_{sf}d_f}{k_f} = C_T \mathrm{Re}^{0.5}\mathrm{Pr}^{0.37}. \quad (13)$$

In Eq. (13), an empiricism has been introduced in the form of the undetermined coefficient C_T. The Reynolds number is based on the cylinder diameter and Pr is the fluid Prandtl number. In applying this correlation, the noncircular cross section of fibers has to be considered. However, upon examination of the Nusselt number correlations for external flow over bodies of varying cross sections ([22]), it appears that the exponent of the Reynolds number has a weak dependence on the cross section. The multiplicative constant in Eq. (13), however, varies considerably. Based on these observations, Zukauskas' correlation has been modified as shown in Eq. (13). Further, it is noted that, in Eq. (13), the Reynolds number is based on the fluid velocity near the fiber. Hence, due to the presence of the solid matrix, its point value is $\mathrm{Re} = (ud_f/\varepsilon\nu)$. The solid-fluid interfacial surface area for arrays of parallel cylinders intersecting in the three mutually perpendicular directions is

$$a_{sf} = \frac{3\pi d_f}{d_p^2}. \quad (14)$$

For metal foams, this expression is modified by taking the structure into account (i.e., open cells shaped like dodecahedra, and noncircular fiber cross-section). By doing so, the values of d_p and d_f, as given in Table 1, are multiplied by 0.59, and $1 - e^{-((1-\varepsilon)/0.04)}$, respectively (see [10], Chapter 1) before being used in Eq. (14).

The transport equations (Eqs. (4)–(6)) are nondimensionalized using $-X = x/H$, $Y = y/H$, $U = u/u_o$, $\theta = (T - T_{in})/\Delta T_{\mathrm{avg}}$ where u_o is the average velocity entering the channel, H is the height of the channel, ΔT_{avg} is the average wall temperature, and T_{in} in the inlet fluid temperature. The resulting equations are

$$\frac{d^2U}{dY^2} = \frac{\varepsilon}{\sqrt{\mathrm{Da}}}(U-1) + \frac{\mathrm{Re}_K}{\mathrm{Da}} f\sqrt{\varepsilon}(U^2-1) \quad (15)$$

$$0 = \frac{1}{\mathrm{Bi}_s}\left(\frac{d^2\theta_s}{dX^2} + \frac{d^2\theta_s}{dY^2}\right) - (\theta_s - \theta_f) \quad (16)$$

$$U\frac{\partial\theta_f}{\partial X} = \frac{\partial}{\partial X}\left(\left(\frac{\mathrm{Da}}{\mathrm{Re}_K\mathrm{Pr}_{fe}} + C_D U\right)\frac{\partial\theta_f}{\partial X}\right) + \frac{\partial}{\partial Y}\left(\left(\frac{\mathrm{Da}}{\mathrm{Re}_K\mathrm{Pr}_{fe}} + C_D U\right)\frac{\partial\theta_f}{\partial Y}\right) + \frac{\mathrm{Bi}_f}{\mathrm{Re}_K\mathrm{Pr}_{fe}}(\theta_s - \theta_f) \quad (17)$$

where

$$\mathrm{Re}_K=\frac{u_o\sqrt{K}}{\nu} \quad \mathrm{Da}=\frac{\sqrt{K}}{H} \quad \mathrm{Bi}_s=\frac{h_{sf}a_{sf}H^2}{k_{se}} \quad \mathrm{Bi}_f=\frac{h_{sf}a_{sf}H\sqrt{K}}{k_{fe}}. \tag{18}$$

Note that Bi_s and Bi_f are not constants but vary along the y-direction, since h_{sf} (Eq. (13)) depends on the velocity. In Eqs. (15)–(18), all quantities except C_D and C_T are known.

The heat dissipation from the heated wall occurs both through the fluid phase and the solid phase. Hence, the total heat transferred can be written as

$$q=\bar{h}L\Delta T_{\mathrm{avg}}=-\int_0^L\left(k_{se}\frac{\partial T_s}{\partial y}+k_{fe}\frac{\partial T_f}{\partial y}\right)dx. \tag{19}$$

Writing Eq. (19) in nondimensional form, an average Nusselt number for the heated surface is

$$\mathrm{Nu}=\frac{\bar{h}L}{k_e}=-\int_0^{L/H}\left(\frac{k_{se}}{k_e}\frac{\partial\theta_s}{\partial Y}+\frac{k_{fe}}{k_e}\frac{\partial\theta_f}{\partial Y}\right)dX. \tag{20}$$

Equation (20) has been formulated to directly compare experimental results with model predictions.

Numerical Procedure

A schematic of the numerical domain is shown in Fig. 5 along with the orientation of the coordinate axes. Numerical boundary conditions are also shown in Fig. 5. For the heated wall, the experimentally determined wall temperature profile is specified. The temperature gradients for both the solid phase and the fluid phase are zero on the insulated wall. At the inlet, the fluid is assumed to enter at the inlet temperature T_{in}. At the exit, a zero diffusion condition is assumed for the fluid phase. This assumption is reasonable, since advection is expected to be the dominant mode of transport in the streamwise (x) direction. The solid phase is assumed to be insulated at both the inlet and the exit.

A fully developed velocity profile is prescribed at the inlet. This velocity profile (function of Y alone) is calculated using the exact solution for the second-order nonlinear ODE, Eq. (15). Following Vafai and Kim [23], the exact solution due to flow through a channel is given by expressing the pressure drop in terms of the center-line velocity. It is reproduced below:

$$U=U_c\left[1-\left(\frac{A+B}{A}\right)(\cosh(D(1-2Y+C)))^2\right]$$

$$A=\varepsilon f\,\mathrm{Re}/6\mathrm{Da}^2 \quad B=\varepsilon/(4\mathrm{Da}^2)+2A \tag{21}$$

$$C=-\frac{1}{D}\mathrm{acosh}\left(\sqrt{\frac{A+B}{A}}\right)-1 \quad D=\sqrt{\frac{A+B}{2}}.$$

Since the average velocity u_o, and not the center-line velocity is known, the center-line velocity had to be guessed and iterated until mass balance was achieved. That is, the integral of the nondimensional velocity over the height of the channel is unity within a specified error of 10^{-5}. This method of calculating the velocity profile was checked by solving the full two-dimensional momentum equation, Eq. (4) in a rectangular domain with an aspect ratio (length to height) of two using the ADI Method of Peaceman and Rachford (see [24]). The fully developed velocity profile obtained from this simulation was identical to the exact solution given by Eq. (21). Since computational time could be saved considerably by using the exact solution, it was employed for all further computations.

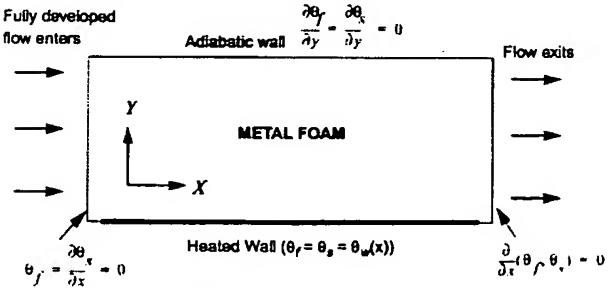

Fig. 5 Schematic of numerical domain with boundary conditions

The energy equations were solved using the ADI finite difference scheme of Peaceman and Rachford ([24]). The convective term in the fluid-phase equation was discretized using first-order upwind differencing for increased stability. The diffusion terms in the solid-phase and fluid-phase equations were discretized using three-point stencils in each direction. To avoid energy balance problems, the numerical domain was extended by five percent at the inlet and the exit. Extensions of 10 percent and 15 percent had no effect on the temperature field or the Nusselt number in the heated section. The equations were marched to asymptotic steady state. The convergence criterion for steady state was that the change in the solid-phase and fluid-phase temperatures was less than 10^{-4} between successive iterations. At steady state, a heat balance within one percent was obtained. A time-step of size 0.03 was found to be an efficient value. While reducing the time-step below this value did not have any effect on the final solution, the convergence rate slowed down.

Grid Dependency and Code Validation

A constant grid spacing was used in the X-direction and a variable grid spacing was used in the Y-direction. The variable grid was laid out in three layers. In Layers I and III, adjacent to the heated and insulated walls, respectively, a constant grid spacing ΔY was used. In Layer II, sandwiched between Layers I and III, a variable grid was used. Table 2 summarizes the results obtained during the grid dependency tests for one of the test samples (see [10], Chapter 4) with $\mathrm{Re}_K=84.1$.

The first column in Table 2 refers to the constant grid spacing ΔY in Layers I and III in the Y-direction. The second and third columns refer to the number of grid points in Layer II and the total number of grid points in the Y-direction, respectively. The fourth column is the number of grid points in the heated section along the X-direction. Based on the grid dependence study, the grid parameters listed in the second row were used for all computations.

In order to validate the code, numerical results were compared to those of Yokoyama and Mahajan [25] as summarized in Table 3. The numerical results ([25]) are indicated within parentheses. Pe* in Table 3 is defined according to ([25]).

Table 2 Results from grid dependency simulations

ΔY	nY2	nY	nXheat	Nu
$5*10^{-4}$	51	63	80	10.97
$2.5*10^{-4}$	51	73	80	11.02
$2.5*10^{-4}$	101	123	80	11.02
$2.5*10^{-4}$	51	73	120	11.02

Table 3 Comparison of numerical results with those in Yokoyama and Mahajan [25]

Pe*	$C_D=0$	$C_D=0.025$
5000	64.9 (64.5)	80.1 (79.4)
7000	75.5 (75.0)	98.5 (97.9)
10000	88.8 (88.1)	123.6 (124.9)

Results and Discussion

Using the numerical code, computations were performed for the conditions of the experiments to verify if the results could be matched in a reasonable manner, and to determine appropriate values for C_D and C_T. The experimental data was collected in the range of nondimensional parameters, $Re_K \sim 11-135$, Da $\sim 5\times10^{-3}-1\times10^{-2}$, and $Pr_e \sim 2.6\times10^{-3}-7.5\times10^{-3}$. Note that the effective Prandtl number values are extremely small compared to the fluid Prandtl number (0.707) due to the high thermal conductivity of the metal foam.

First, the condition of zero dispersion (i.e., $C_D=0$) was studied. Figure 6 shows a plot of the Nusselt number as a function of $Re_K Pr_e$ for different values of C_T with $C_D=0$. The results are for Sample 2, and the experimental points are shown by the solid symbols. As expected, the Nusselt number increases with increase in C_T since the efficiency of heat transfer between the two phases improves. However, note that there is practically no difference in the computed results for $C_T>0.52$ indicating that the phases are close to the thermal equilibrium condition. Figure 7 shows the variation of the temperature profile along the transverse direction at the midplane for three different Reynolds numbers. Note that the adiabatic wall temperature (i.e., the wall temperature at $Y=1$) for the solid and fluid phases is not the same as the ambient temperature for all three values of Re_K. However, as Re_K increases, the adiabatic wall temperature approaches the ambient temperature. The indication is that the thermal boundary layer at the heated wall decreases with increase in Re_K.

To understand the relative magnitudes of the various transport phenomena, it is useful to examine the solid and fluid-phase heat transfer rates at the heated wall. In Fig. 8, the local variations of the nondimensional heat transfer rates (the two components of Eq. (20)) are plotted. Clearly, the fluid-phase component accounts for a negligibly small portion of the total heat rate. Further, its local value decreases rapidly along the streamwise direction. This can be explained as follows. The predominant mode of transport from the heated surface to the fluid is by conduction through the solid phase and interfacial heat transfer from the solid to the fluid phase. Due to the efficient interfacial heat transfer, the fluid temperature is close to the solid temperature. This has an effect of decreasing the fluid temperature gradient at the wall (by thickening the boundary layer), and consequently the local heat transfer rate. Further, since the fluid conductivity is much smaller than the solid conductivity, the net heat transferred from the wall to the fluid is low.

In the numerical results presented so far, thermal dispersion has not been taken into account. It can be seen from the plot in Fig. 8 that the heat transferred directly to the fluid from the heated wall is negligible compared to the heat transferred interfacially from the solid to the fluid. Hence, the dispersion phenomenon that primarily enhances the wall heat transfer, is expected to be low. Figure 9 shows a plot of the total Nusselt number as a function of $Re_K Pr_e$ for Sample 2. The plots are for two different values of C_T as shown in the figure. For each C_T value, two lines are shown. They are the results of numerical simulations with and without the inclusion of dispersion effects. For the simulations for which dis-

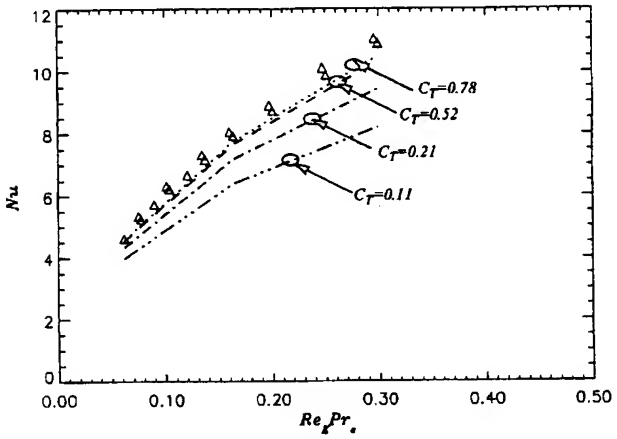

Fig. 6 Nu as a function of $Re_K Pr_e$ for different values of C_T. Data are for Sample 2.

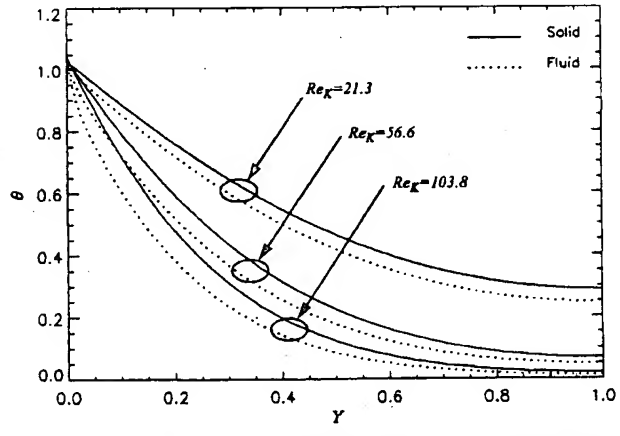

Fig. 7 Nondimensional temperature along the transverse direction. $C_T=0.52$, Sample 2.

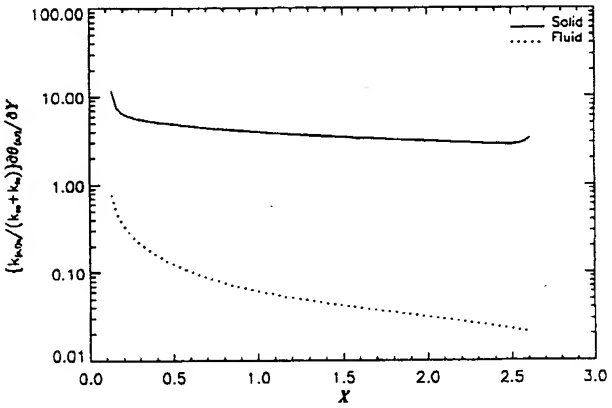

Fig. 8 Solid and fluid phase local heat transfer rate. Sample 2, $Re_K=103.8$.

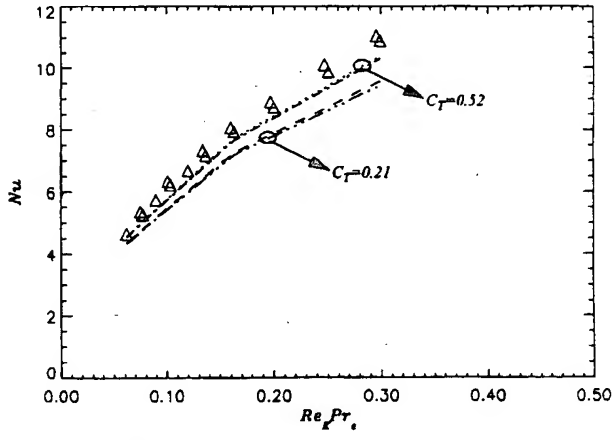

Fig. 9 Nu as a $Re_K Pr_e$ with dispersion effect included ($C_D=0.1$). Data is for Sample 2.

Table 4 Characteristics of foam samples used in Hunt and Tien [2]

No.	Material	ε	d_p (cm)	$K*10^7$ (m^2)	f	k_{se} (W/m-K)	k_{fe} (W/m-K)
H1	C	0.97	0.2	4.1	0.11	0.073	0.58
H2	C	0.97	0.1	0.92	0.077	0.073	0.58
H3	Ni	0.97	0.1	0.96	0.089	0.854	0.579
H4	Al	0.97	0.2	4.8	0.17	2.19	0.579
H5	Al	0.94	0.25	17.0	0.30	3.84	0.558

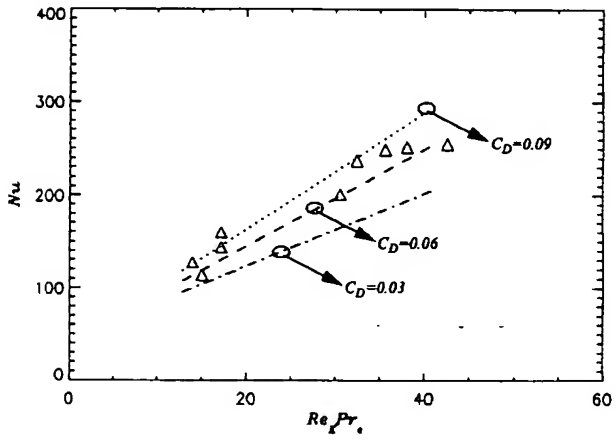

Fig. 10 Nusselt number as a function of $Re_K Pr_e$ for different values of C_D (Sample H3)

persion effects were included, a value $C_D = 0.1$ was used. As it is evident from the figure, dispersion has no significant effect on the total transport. This is immediately clear by re-examining the thermal dispersion model postulated earlier,

$$\frac{k_d}{k_e} = C_D(\mathrm{Re}_K \mathrm{Pr}_e). \tag{22}$$

For k_d to have any significant effect on the overall transport, it must be at least of the same order of magnitude as k_e. For a typical value of $\mathrm{Re}_K \mathrm{Pr}_e = 0.3$, and $C_D = 0.1$, k_d is merely three percent of the total stagnant thermal conductivity. Although its value is still *seven* times higher than the fluid conductivity, the effect on the overall transport is negligible because, as mentioned before, the dominant mode of transport is by conduction through the solid phase and interfacial convection, which is largely unaffected by dispersion. The value, $C_D = 0.1$, used for illustrating this is not entirely arbitrary. It is based on order of magnitude estimates in ([7]). In any case, it is clear that it is difficult to accurately quantify dispersion effects when the solid-phase conductivity is much larger than its fluid-phase counterpart, as is the case here.

Although an accurate estimate of C_D cannot be made by using the metal foam-air experiments, an estimate of C_T is possible. From Fig. 9, it is seen that a good match of the data with the numerical results is obtained with $C_T = 0.52$. This value is representative of heat transfer from cylinders in crossflow ([21]). Further, as will be seen later, this value of C_T is sufficient to model forced convection transport in metal foams with water as the fluid phase. We note here that a two-equation model for energy may not be necessary for all combinations of experimental data. However, a detailed study that establishes bounds for nondimensional parameters for which two-equation analyses are necessary may be useful for application to practical situations (see, for example, [26]).

The only other experimental and theoretical work that addresses forced convection in metal foams is that of Hunt and Tien [2]. Their study used foams made of aluminum, nickel, carbon, with water as the fluid phase. Hence, the fluid conductivity is not a negligible fraction of the effective conductivity. Consequently, dispersion effects are expected to be much higher. Although an error was found in the numerical calculations (which eventually led to the conclusion that $C_D = 0.025$), the experiments seemed to be in order. Of the seven samples used in their experiment, five representative samples were chosen for analysis here (see Table 4). The conductivities in the last two columns of Table 4 were evaluated using the expressions developed in this study (Eqs. (9),(10)). Since water was used as the fluid phase, interfacial heat transfer was efficient and all samples satisfied local thermal equilibrium conditions as expected. ($C_T = 0.52$ was used for the computations, based on the aluminum-air study described earlier.)

To study the dispersion effect numerically, Sample H3 was chosen for investigation. The average heat transfer coefficients were extracted from their experimental Nusselt numbers and used here for comparison. The computed Nusselt numbers for different values of the dispersion coefficient, C_D, are shown in Fig. 10 along with the experimental data. A reasonable fit is obtained for $C_D = 0.06$. As expected, and unlike in the aluminum foam-air

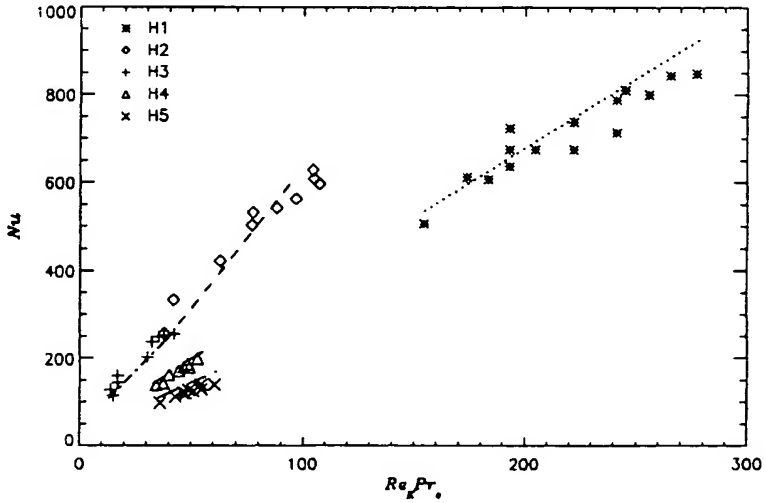

Fig. 11 Comparison of numerical simulations (this study) with the experimental results in Hunt and Tien [2] for samples in Table 4

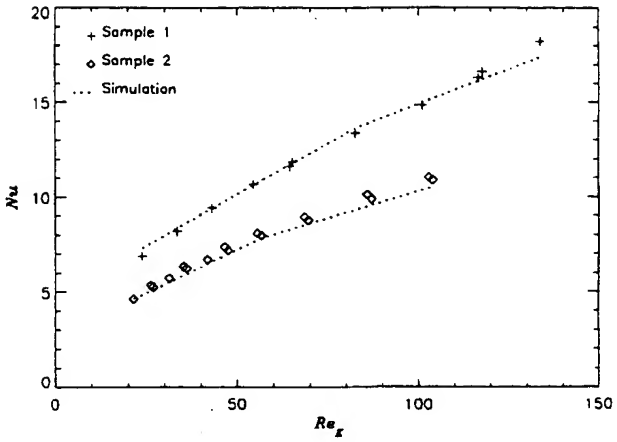

Fig. 12 Nusselt number as a function of Re_K for the five PPI samples (Table 1)

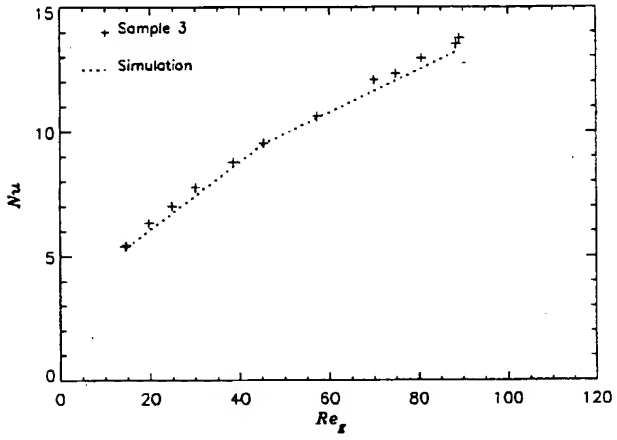

Fig. 13 Nusselt number as a function of Re_K for the ten PPI samples (Table 1)

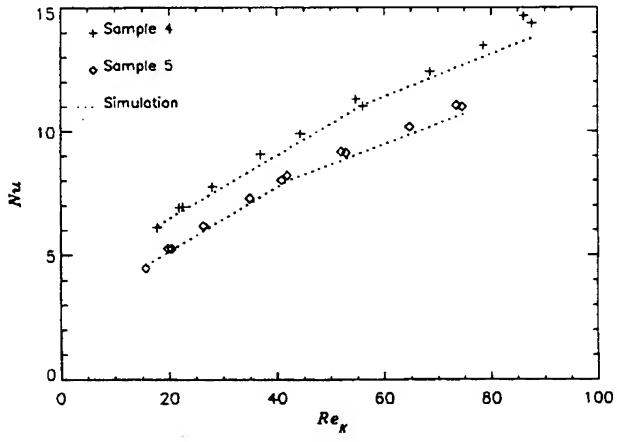

Fig. 14 Nusselt number as a function of Re_K for the 20 PPI samples (Table 1)

combination used in this study, the dispersion effect is considerable here. In this particular case, heat transfer enhancement due to dispersion is almost 80 percent. Using Eq. (22), and a representative value of $Re_K Pr_e = 30$, the dispersion conductivity is calculated to be 175 percent of the stagnant conductivity. This is a significant

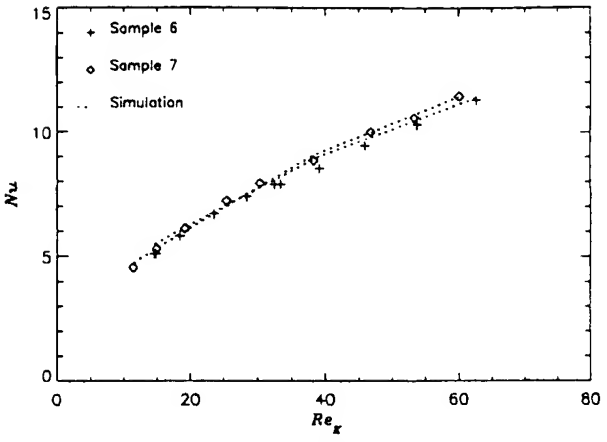

Fig. 15 Nusselt number as a function of Re_K for the 40 PPI samples (Table 1)

enhancement compared to the low value of three percent obtained earlier for the aluminum-air combination. The experimental results in ([2]) are plotted in Fig. 11 for a thermal dispersion coefficient value of 0.06. A good fit is obtained for all samples, suggesting that $C_D = 0.06$ is appropriate.

By analyzing the data collected in this study for foam-air combinations, and that published in Hunt and Tien [2] for foam-water combinations, the coefficients C_T and C_D values of 0.52, and 0.06 seem reasonable. As a last check, numerical simulations were performed for the same experimental conditions of all samples (Table 1) used in the present study. The results of these simulations are plotted in Figs. 12–15 as a function of the Reynolds number, along with the experimental data. Once again, a very good fit with the experimental data is obtained confirming the values of C_D and C_T to be good. However, the following point is noted. There appears to be a systematic deviation between the experimental and computed results for high Reynolds number. In particular, the numerical results appear to underpredict the experimental Nusselt number for $Re_K > 80$. The indication is that some other transport enhancing effect (e.g., turbulence) may be taking effect. No such systematic deviation is observed in the experimental results of Hunt and Tien [2]. However, the maximum Reynolds number in that study was around 60.

Summary

A detailed study of forced convection in metal foams has been performed. The goal of the study was to quantify thermal dispersion and thermal nonequilibrium effects in metal foams. To this end, both experimental and numerical methods were employed. Experiments were performed with a wide variety of aluminum metal foams. Results indicate that for foam-air combinations, the transport enhancing effect of thermal dispersion is extremely low due to the relatively high conductivity of the solid matrix. However, for foam-water combinations, ours and past available results indicate that thermal dispersion can be very high and accounts for bulk of the transport.

A thermal nonequilibrium model was used in all cases. The values $C_T = 0.52$, and $C_D = 0.06$ were found to be appropriate. Currently, forced convection transport in foamed materials is being studied using foams of other materials (carbon, copper) along with various fluids (air, water, FC-72) in order to reconfirm the results of the present study. Those findings will appear in a future publication.

Acknowledgments

This work was funded by CAMPmode at the University of Colorado. The authors wish to thank Dr. Yoichi Yokoyama for

helpful discussions and Mr. Bryan Leyda of ERG, Inc. for providing the experiment samples and for discussions at various stages of this work.

Nomenclature

a_{sf} = specific solid-fluid interfacial surface area (m^{-1})
Bi_f = $h_{sf}a_{sf}H\sqrt{K}/k_{fe}$, fluid-phase effective Biot number
Bi_s = $h_{sf}a_{sf}H^2/k_{se}$, solid-phase effective Biot number
C_D = coefficient of thermal dispersion
C_T = coefficient in Eq. (13)
Da = $\sqrt{K}/H$, Darcy number
f = inertia coefficient
h_{sf} = interfacial heat transfer coefficient (W/m^2-K)
K = permeability (m^2)
Pr_e = $\mu c_p/k_e$, Prandtl number based on effective conductivity
q = heat input to patch heaters (W)
Re_K = $u_o\sqrt{K}/\nu$, Reynolds number based on permeability
T_{in} = measured fluid temperature (before entering heated section) (°C)
T_{amb} = measured fluid temperature (before entering unheated section) (°C)
T_{wi} = measured wall temperatures (°C)
ΔT_{avg} = average wall temperature with respect to fluid inlet temperature, T_{in}
u_o = measured average flow velocity entering foam sample (m/s)

Greek Symbols

θ = $(T-T_{in})/(\Delta T_{avg})$

Subscripts

d = dispersive
e = effective

References

[1] Kaviany, M., 1991, *Principles of Heat Transfer in Porous Media*, Springer-Verlag, New York.
[2] Hunt, M. L., and Tien, C. L., 1988, "Effects of Thermal Dispersion on Forced Convection in Fibrous Media," Int. J. Heat Mass Transf., 31, pp. 301–309.
[3] Sathe, S. B., Peck, R. E., and Tong, T. W., 1990, "A Numerical Analysis of Heat Transfer and Combustion in Porous Radiant Burners," Int. J. Heat Mass Transf., 33, No. 6, pp. 1331–1338.
[4] Lee, Y. C., Zhang, W., Xie, H., and Mahajan, R. L., 1993, "Cooling of a FCHIP Package With 100 W, 1 cm^2 Chip," *Proceedings of the 1993 ASME Int. Elec. Packaging Conf.*, Vol. 1, ASME, New York, pp. 419–423.
[5] Calmidi, V. V., and Mahajan, R. L., 1999, "The Effective Thermal Conductivity of High Porosity Fibrous Metal Foams," ASME J. Heat Transfer, 121, pp. 466–471.
[6] Bhattacharya, A., Calmidi, V. V., and Mahajan, R. L., 1999, "An Analytical-Experimental Study for the Determination of the Effective Thermal Conductivity of High-Porosity Fibrous Foams," *ASME IMECE '99*, ASME, New York, pp. 13–20.
[7] Koch, D. L., and Brady, J. F., 1986, "The Effective Diffusivity of Fibrous Media," AIChE J., 32, pp. 575–591.
[8] Hsu, C. T., and Cheng, P., 1990, "Thermal Dispersion in Porous Media," Int. J. Heat Mass Transf., 33, No. 8, pp. 1587–1597.
[9] Adnani, P., Catton, I., and Abdou, M. A., 1995, "Non-Darcian Forced Convection in Porous Media With Anisotropic Dispersion," ASME J. Heat Transfer, 117, pp. 447–451.
[10] Calmidi, V. V., 1998, "Transport Phenomena in High Porosity Metal Foams," Ph.D. thesis, University of Colorado, Boulder, CO.
[11] Beavers, G. S., and Sparrow, E. M., 1969, "Non-Darcy Flow Through Fibrous Porous Media," ASME J. Appl. Mech., 36, pp. 711–714.
[12] Vafai, K., and Tien, C. L., 1981, "Boundary and Inertial Effects on Flow and Heat Transfer in Porous Media," Int. J. Heat Mass Transf., 24, pp. 195–203.
[13] DuPlessis, P., Montillet, A., Comiti, J., and Legrand, J., 1994, "Pressure Drop Prediction for Flow Through High Porosity Metallic Foams," Chem. Eng. Sci., 49, pp. 3545–3553.
[14] Carbonell, R. G., and Whitaker, S., 1984, "Heat and Mass Transfer in Porous Media," *Fundamentals of Transport Phenomena in Porous Media*, Bear and Corapcioglu, eds., Martinus Nijhoff, Dordrecht, The Netherlands, pp. 121–198.
[15] Kaviany, M., 1994, *Convective Heat Transfer*, Springer-Verlag, New York.
[16] Zanotti, F., and Carbonell, R. G., 1984, "Development of Transport Equations for Multiphase System-III," Chem. Eng. Sci., 39, pp. 299–311.
[17] Wakao, N., Kaguei, S., and Funazkri, T., 1979, "Effect of Fluid Dispersion Coefficients on Particle-to-Fluid Heat Transfer Co-efficients in Packed Beds," Chem. Eng. Sci., 34, pp. 325–336.
[18] Hwang, G. J., and Chao, C. H., 1994, "Heat Transfer Measurements and Analysis for Sintered Porous Channels," ASME J. Heat Transfer, 117, pp. 725–732.
[19] Cheng, P., and Vortmeyer, D., 1988, "Transverse Thermal Dispersion and Wall Channelling in a Packed Bed With Forced Convective Flow," Int. J. Heat Mass Transf., 43, No. 9, pp. 2523–2532.
[20] Koch, D. L., 1996, "Hydrodynamic Diffusion Near Solid Boundaries With Applications to Heat and Mass Transport Into Sheared Suspensions and Fixed-Fibre Beds," J. Fluid Mech., 318, pp. 31–47.
[21] Zukauskas, A. A., 1987, "Convective Heat Transfer in Cross-Flow," *Handbook of Single-Phase Heat Transfer*, Kakac, S., et al., eds. Wiley, New York.
[22] Incropera, F. P., and DeWitt, D., 1997, *Fundamentals of Heat and Mass Transfer*, Wiley, New York.
[23] Vafai, K., and Kim, S. J., 1989, "Forced Convection in a Channel Filled with a Porous Medium: An Exact Solution," ASME J. Heat Transfer, 111, pp. 1103–1106.
[24] Roache, P. J., 1982, *Computational Fluid Dynamics*, Hermosa, Albuquerque, NM.
[25] Yokoyama, Y., and Mahajan, R. L., 1995, "Non-Darcian Convective Heat Transfer in a Horizontal Duct," *Proceedings of the National Heat Transfer Conference*, Vol. 7, ASME, New York, pp. 83–92.
[26] Amiri, A., and Vafai, K., 1994, "Analysis of Dispersion Effects and Local Thermal Non-Equilibrium, Non-Darcian, Variable Porosity Incompressible Flow Through Porous Media," Int. J. Heat Mass Transf., 37, pp. 939–954.